Title

Small pretreatment lesion size and high sphericity as favorable prognostic factors after laser interstitial thermal therapy in brain metastases.

Journal

Journal of Neurosurgery, 140(2)

ISSN

0022-3085

Authors

Sanvito, Francesco
Telesca, Donatello
Cho, Nicholas S
et al.

Publication Date

2024-02-01

DOI

10.3171/2023.5.jns23285

Peer reviewed

HHS Public Access

Author manuscript

J Neurosurg. Author manuscript; available in PMC 2025 February 02.

Published in final edited form as:

J Neurosurg. 2024 February 01; 140(2): 338–349. doi:10.3171/2023.5.JNS23285.

Small pretreatment lesion size and high sphericity as favorable prognostic factors after laser interstitial thermal therapy in brain metastases

Francesco Sanvito, MD[1,2,5], **Donatello Telesca, PhD**[6], **Nicholas S. Cho, BS**[1,2,7,8], **Jessica T. Sayari, BA**[1,2], **Raksha Nagaraj, MS**[1,2], **Catalina Raymond, MSc**[1,2], **Shivam Rana**[1,2,3], **Kunal Patel, MD**[3], **Khashayar Mozaffari, BS**[3], **Ansley A. Unterberger, BS**[3], **Negar Khanlou, MD**[9], **Shino Magaki, MD, PhD**[9], **Nader Pouratian, MD, PhD**[10], **Richard G. Everson, MD**[3], **Isaac Yang, MD**[11,12,13,14,15,16], **Won Kim, MD**[3], **Benjamin M. Ellingson, PhD**[1,2,3,4,7]

[1]UCLA Brain Tumor Imaging Laboratory (BTIL), Center for Computer Vision and Imaging Biomarkers, University of California, Los Angeles

[2]Department of Radiological Sciences, University of California, Los Angeles, California

[3]Department of Neurosurgery, University of California, Los Angeles, California

[4]Department of Psychiatry and Biobehavioral Sciences, David Geffen School of Medicine, University of California, Los Angeles, California

[5]Department of Clinical, Surgical, Diagnostic, and Pediatric Sciences, Unit of Radiology, University of Pavia, Italy

[6]Department of Biostatistics, University of California, Los Angeles

[7]Department of Bioengineering, Henry Samueli School of Engineering and Applied Science, University of California, Los Angeles

[8]Medical Scientist Training Program, David Geffen School of Medicine, University of California, Los Angeles

Correspondence Benjamin M. Ellingson: University of California, Los Angeles, CA. bellingson@mednet.ucla.edu.

Author Contributions

Conception and design: Ellingson, Sanvito, Yang, Kim, Everson. Acquisition of data: Ellingson, Sanvito, Mozaffari, Unterberger, Pouratian, Everson, Kim, Yang. Analysis and interpretation of data: Ellingson, Sanvito, Cho, Nagaraj, Sayari, Rana, Yang. Drafting the article: Sanvito. Critically revising the article: Ellingson, Sanvito, Cho, Sayari, Patel, Mozaffari, Unterberger, Pouratian, Everson, Yang, Kim. Reviewed submitted version of manuscript: Ellingson, Sanvito, Cho, Sayari, Nagaraj, Rana, Patel, Mozaffari, Unterberger, Khanlou, Magaki, Pouratian, Everson, Yang, Kim. Approved the final version of the manuscript on behalf of all authors: Ellingson. Statistical analysis: Sanvito, Telesca. Administrative/technical/material support: Ellingson, Sanvito, Raymond. Study supervision: Ellingson, Yang, Kim, Everson. Histopathology analysis and diagnosis: Khanlou, Magaki.

Disclosures

Dr. Pouratian reported personal fees from Brainlab, Abbott Laboratories, Boston Scientific, and Sensoria Therapeutics outside the submitted work. Dr. Kim reported personal fees from Monteris during the conduct of the study. Dr. Ellingson reported personal fees from Monteris outside the submitted work.

Supplemental Information

Online-Only Content

Supplemental material is available with the online version of the article.

Supplemental Table and Figures. https://thejns.org/doi/suppl/10.3171/2023.5.JNS23285.

Previous Presentations

Preliminary analyses on these data sets were previously presented at the Society for Neuro-Oncology Annual Meeting, November 16–20, 2022, in Tampa, Florida.

[9]Department of Pathology and Laboratory Medicine, Section of Neuropathology, David Geffen School of Medicine, University of California, Los Angeles, California

[10]Department of Neurological Surgery, UT Southwestern Medical Center, Dallas, Texas

[11]Department of Neurosurgery, Ronald Reagan UCLA Medical Center, University of California, Los Angeles

[12]Department of Head and Neck Surgery, Ronald Reagan UCLA Medical Center, University of California, Los Angeles

[13]Department of Radiation Oncology, Ronald Reagan UCLA Medical Center, University of California, Los Angeles

[14]David Geffen School of Medicine, Ronald Reagan UCLA Medical Center, University of California, Los Angeles

[15]Jonsson Comprehensive Cancer Center, Ronald Reagan UCLA Medical Center, University of California, Los Angeles

[16]Los Angeles Biomedical Research Institute (LA BioMed) at Harbor-UCLA Medical Center, University of California, Los Angeles, California

Abstract

OBJECTIVE—The objective of this study was to identify baseline clinical and radiological characteristics of brain metastases (BMs) associated with a higher probability of lesion-specific progression-free survival (PFS-L) after laser interstitial thermal therapy (LITT).

METHODS—A total of 47 lesions in 42 patients with BMs treated with LITT were retrospectively examined, including newly diagnosed BM, suspected recurrent BM, and suspected radiation necrosis. The association of baseline clinical and radiological features with PFS-L was assessed using survival analyses. Radiological features included lesion size measurements, diffusion and perfusion metrics, and sphericity, which is a radiomic feature ranging from 1 (perfect sphere) to 0.

RESULTS—The probability of PFS-L for the entire cohort was 88.0% at 3 months, 70.6% at 6 months, 67.4% at 1 and 2 years, and 62.2% at 3 years. For lesions progressing after LITT (n = 13), the median time to progression was 3.9 months, and most lesions (n = 11) progressed within 6 months after LITT. In lesions showing response to LITT (n = 17), the median time to response was 12.1 months. All 3 newly diagnosed BMs showed a long-term response. The mean (± SD) follow-up duration for all censored lesions (n = 34) was 20.7 ± 19.4 months (range 12 days to 6.1 years). The mean pretreatment enhancing volume was 2.68 cm3 and the mean sphericity was 0.70. Pretreatment small enhancing volume ($p = 0.003$) and high sphericity ($p = 0.024$) computed from lesion segmentation predicted a longer PFS-L after LITT. Lesions meeting optimal cutoffs of either enhancing volume < 2.5 cm^3 (adjusted $p = 0.004$) or sphericity ≥ 0.705 (adjusted $p = 0.019$) had longer PFS-L, and their probability of PFS-L was 86.8% at 3 years. Lesions meeting both cutoffs showed a cumulative benefit ($p < 0.0001$), with a 100% probability of PFS-L at 3 years, which was unchanged at the end of follow-up (4.1 years). Manually computed estimates of lesion size (maximal axial diameter, $p = 0.011$) and sphericity ($p = 0.043$) were also predictors of PFS-L. Optimal cutoffs of diameter < 2 cm (adjusted $p = 0.035$) or manual sphericity ≥ 0.91 (adjusted p =

0.092) identified lesions with longer PFS-L, and lesions meeting both cutoffs showed a cumulative benefit (p = 0.0023). Baseline diffusion imaging did not predict PFS-L. A subset of lesions (n = 7) with highly perfused hotspots had worse PFS-L (adjusted p = 0.010), but perfusion signal contamination from vessels and cortex and underlying size differences were possible confounders.

CONCLUSIONS—Small size and high sphericity are ideal baseline features for lesions considered for LITT treatment, with a cumulative PFS-L benefit when both features are present, that could aid patient selection.

Keywords

laser interstitial thermal therapy; LITT; brain metastases; neurooncology; radiation necrosis; patient selection; oncology

---

The treatment of brain metastases (BMs) primarily relies on local therapy, regardless of the presence of symptoms and the administration of systemic treatments, according to the recent American Society for Clinical Oncology/Society for Neuro-Oncology/American Society for Radiation Oncology guidelines for the clinical management of BMs.[1] Depending on the size, number, and location of the lesions, the most commonly adopted local therapies are stereotactic radiosurgery (SRS) and/or resection.[1]

Although local treatments can achieve local disease control, the disease recurrence rate at 1 year has been estimated as approximately 14%.[2] A concern for BM recurrence should be raised in the presence of an enlarging contrast-enhancing lesion in the site of a previously treated BM, as documented on MRI. Alternatively, such enhancing tissue may represent radiation necrosis (RN; as opposed to neoplastic disease), which has been reported to occur in 8%–20% of SRS-treated BMs.[3] Although many cases of RN are self-limiting, this condition can be symptomatic and require treatment, including steroids to reduce inflammation-mediated manifestations and vasogenic edema inducing mass effect.[4] When BM recurrence is suspected, repeat radiation and/or surgery is not always ideal. Repeat radiation treatment is often debatable due to the concern for cumulative adverse effects.[5] Surgery may be contraindicated for deep-seated locations or in patients with comorbidities.[6,7] Therefore, new strategies for the local treatment of recurrent BMs have been explored.

Laser interstitial thermal therapy (LITT) represents a novel option for the local treatment of both BM and RN,[4] consisting of a stereotactic MRI-guided heat-induced ablation.[8,9] After the tip of an intracranial catheter is positioned within the target lesion, a neodymium-doped yttrium aluminum garnet (Nd:YAG) laser is applied to achieve heat-induced tissue damage.[4] Cell damage and/or coagulative necrosis can be achieved depending on the time and duration of the laser application.[5,10] During the procedure, a dedicated MRI sequence is used to monitor voxel-wise temperature changes[11] with the MR thermometry technique.[12]

LITT is a minimally invasive treatment compared with open surgery, with similar efficacy and a shorter hospitalization time.[6] Because SRS and surgery are still considered the main indications for a newly diagnosed BM, LITT is mostly used in the recurrent setting[6,13-18] where it combines a diagnostic and therapeutic function. As a diagnostic

function, LITT offers the possibility to gather lesion tissue for histopathological evaluation using stereotactic biopsy before the procedure, to distinguish recurrent BM from RN.[4] As a therapeutic option, LITT can effectively treat both BM and RN,[4,19-21] resulting in local disease control, clinical benefit, and symptom improvement for both BM and RN cases.[17,22]

Although LITT is a promising local treatment option, evidence supporting definitive recommendations for or against this procedure remain insufficient.[1] Specifically, literature providing criteria for patient selection to maximize the success of this treatment is scarce. In this study, we aim to assess the predictive value of clinical and radiological baseline characteristics of LITT-treated lesions—including size, shape, and advanced imaging features—and to propose optimized cutoffs for the evaluated metrics to aid patient selection in the clinical setting.

Methods

Patient Selection and Clinical Characteristics

Lesions treated at our institution between June 2014 and August 2021 were retrospectively reviewed. Patient inclusion criteria for the study were as follows: 1) diagnosis of BM; 2) received LITT in either the newly diagnosed or recurrent setting (for suspicion of either recurrent BM or RN); and 3) availability of baseline pre-LITT and follow-up MR images. Baseline clinical characteristics were annotated, including age, sex, primary tumor, date and type of prior local treatments, neurological symptoms, and administration of systemic therapy from 3 months before to 3 months after LITT. Patients provided written informed consent to be part of the database approved by the IRB at the University of California, Los Angeles.

Surgical Procedure

LITT was performed using either the Visualase Thermal Therapy system (Visualase, Inc.) or the Monteris Medical NeuroBlate system (Monteris Medical, Inc.). Patients were placed in Mayfield head clamps and registered to recent MR images using Curve intraoperative neuronavigation software (Brainlab surgical navigation system). A preplanned trajectory (Brainlab Elements and Varioguide) was used to guide the placement of the laser fiber. In a subset of patients, stereotactic biopsy was performed prior to ablation for histopathological evaluation. During LITT, thermal changes in brain tissue were monitored through MR thermometry. Ablation was deemed sufficient with maximal safe ablation of contrast-enhancing tissue sparing the surrounding healthy tissue.

Imaging Acquisition and Analysis

The baseline (pre-LITT) MRI protocol included T1-weighted images before (T1) and after (CET1) contrast agent administration, diffusion-weighted imaging (DWI), and dynamic susceptibility contrast (DSC) perfusion imaging. The apparent diffusion coefficient (ADC) was computed on the scanner from DWI. After motion correction, normalized relative cerebral blood volume (nrCBV) maps were computed from DSC imaging using a bidirectional leakage correction algorithm[23] and a normalization to the cerebral median relative cerebral blood volume. T1-weighted images, ADC, and nrCBV were registered to

CET1 using the *flirt* function from the FMRIB software library (FSL; University of Oxford; https://fsl.fmrib.ox.ac.uk/fsl/).

A 3D segmentation representing the volume of the contrast-enhancing lesion (CE_{vol}) was obtained by manually contouring the lesion at each time point and quantitatively thresholding voxels exhibiting contrast enhancement on T1 subtraction images.[24] An additional whole-lesion segmentation included non–contrast-enhancing portions as well, typically representing the cystic/necrotic core. Perilesional edema was not included in the segmentations. The following quantitative values were extracted from CE_{vol}: median ADC, median nrCBV, 10th percentile ADC, and 90th percentile nrCBV. Whole-lesion sphericity (ψ), a radiomic feature ranging from 1 (perfect sphere) to 0, was computed using pyradiomics (https://www.radiomics.io/pyradiomics.html).

A neuroradiologist with 6 years of experience in neuroimaging (F.S.) annotated lesion location, quality-checked all image registrations, manually refined segmentations, and annotated three baseline diameters: maximal diameter in the axial plane (d_{ax1}), maximal perpendicular diameter in the axial plane (d_{ax2}), and maximal vertical diameter (perpendicular to the axial slices; d_{vert}). These three manual diameters were used to compute a manually derived approximated sphericity (ψ_{manual}):

$$\psi_{manual} = \frac{\sqrt[3]{36\pi V_{estimated}^{2}}}{S_{estimated}}$$

where $V_{estimated}$ and $S_{estimated}$ were the estimated volume and surface of the lesion when approximated to an ellipsoid:

$$V_{estimated} = (4 / 3)\pi(d_{ax1} / 2)(d_{ax2} / 2)(d_{vert} / 2)$$

$$S_{estimated} = 4\pi \sqrt[1.6]{\frac{\left(\frac{d_{ax1}}{2}\frac{d_{ax2}}{2}\right)^{1.6} + \left(\frac{d_{ax1}}{2}\frac{d_{vert}}{2}\right)^{1.6} + \left(\frac{d_{vert}}{2}\frac{d_{ax2}}{2}\right)^{1.6}}{3}}$$

To estimate the extent of ablation, the immediate post-LITT CET1 was registered to pre-LITT CET1, both CET1 were normalized, and a subtraction image depicting the outer rim of the ablated volume was generated, as proposed in a previous study.[14] The pre-LITT whole-lesion segmentation was superimposed onto the subtraction image to assess whether the pretreatment lesion was included in the ablation rim. The ablation was considered complete only when a complete ablation rim surrounded the pre-LITT whole-lesion segmentation. This method, along with representative cases, is illustrated in Suppl. Fig. 1.

Treatment Response Assessment

We assessed LITT response in terms of lesion-specific progression-free survival (PFS-L), which only evaluates treatment response in the treated lesion, as proposed in other studies.[14]

The volumetric thresholds (expressed in percentages) proposed in the modified Response Assessment in Neuro-Oncology (mRANO) criteria were adopted.[25] Unlike the RANO-BM criteria,[26] the mRANO criteria provide volumetric thresholds for response and progression.

Lesions were followed until progressive disease (PD) was noted or they were censored. Treatment response was defined as a ≥ 65% CE_{vol} shrinkage compared with baseline, confirmed on two MRI scans over 4 weeks. Lesions meeting response criteria after 12 months were considered long-term responders (LTRs). PD was defined as a ≥ 40% CE_{vol} increase compared with baseline or nadir, either confirmed by an additional subsequent ≥ 40% CE_{vol} increase after 4 weeks or followed by a clinical decision to re-treat the disease or control symptoms. PD was subdivided into early (< 6 months from LITT) and late (6–12 months) PD. Long-term disease control (LTDC) was defined as a 12-month follow-up without progression or response, including stable disease and progression after 12 months. Pseudoprogression was defined according to mRANO criteria,[25] including cases with a ≥ 40% CE_{vol} increase without an additional subsequent ≥ 40% CE_{vol} increase after 4 weeks.

A visual map of the locations of all lesions in the Montreal Neurological Institute (MNI) space was generated. The map was obtained by registering segmentations to the normalized MNI space with a concatenation of linear (FSL *flirt*) and nonlinear (FSL *fnirt*) transformations as previously described,[27] and then was color-coded according to treatment response.

Statistical Analyses

Statistical analyses were performed using Prism software (version 9.0.0 for Mac OS, GraphPad Software; www.graphpad.com). A p value threshold < 0.05 was used for significance. Survival analyses assessing relationships between baseline variables and PFS-L were performed with a log-rank test for categorial variables, log-rank test for trend for categorial ordinal variables, and Cox proportional hazards regression analysis for continuous variables. An in-house MATLAB script (MathWorks) was used to achieve optimal thresholds of continuous variables for a log-rank analysis by computing p values and hazard ratios (HRs) while looping through values as previously described.[28,29] The obtained p values were adjusted for significance testing for the maximal HR, as described in Lausen and Schumacher.[30] Group differences in categorial variables were evaluated with a Mann-Whitney U-test. The correlation between continuous variables was evaluated with a Pearson correlation or, when appropriate, nonlinear regressions (e.g., logarithmic fit). To assess the equivalence between manually derived sphericity and sphericity, a test of equivalence was conducted using a union intersection test, the null hypothesis being slope ≠ 1 and intercept ≠ 0 in a linear regression. Logistic regression was used to evaluate the association between the continuous variables of interest and the extent of ablation (complete or incomplete).

Results

Patient Selection and Baseline Characteristics

We evaluated 47 lesions across 42 patients (5 patients had 2 lesions treated). Table 1 summarizes the baseline clinical characteristics of lesions and patients. Three lesions were newly diagnosed and 44 were recurrent. The recurrent lesions were previously treated with SRS alone and/or with resection plus cavity stereotactic body radiation therapy (RT; 30 Gy in 5 fractions)—except for 3, treated with surgery alone, whole-brain RT alone, and hypofractionated RT alone, respectively. Baseline symptoms included seizures, motor function impairment (hemiparesis, lateralized hyposthenia, impaired gait), lateralized hypoesthesia, visual field disturbances, dysonjugate gaze, language disturbances, memory loss, and persistent headache. No lesions received consolidation SRS after LITT. Table 2 summarizes the baseline radiological characteristics of the lesions.

Surgical Procedure

LITT was performed using two catheters in 5 cases (10.6%) and using one catheter in 42 cases (89.4%). Two patients experienced complications linked to pin site infection, both successfully managed using oral antibiotics. Four patients had mild worsening of preexisting focal neurological symptoms such as visual deficits, gait disturbances, and hypoesthesia. Ablation was estimated as complete in 15 lesions (31.9%) and incomplete in 32 (68.1%); the method used to estimate the extent of ablation was very conservative (discussed below).

Treatment Response Assessment: Descriptive Statistics

Table 3 reports treatment response assessment. Thirtyseven lesions (78.7%) showed a transitory growth meeting the criteria for pseudoprogression immediately after LITT. The probability of PFS-L for the whole cohort was 88.0% at 3 months, 70.6% at 6 months, 67.4% at 1 and 2 years, and 62.2% at 3 years. The median time to progression was 3.9 months (range 0.8–27.9 months; n = 13 with PD), and early PD (n = 11) was more common than PD after 6 months (n = 2). The median time to response was 12.1 months (range 2.8–22.5 months; n = 17 responding lesions). All responding lesions still met the criteria for treatment response at the time of censoring, and approximately half of these (n = 8) were followed for ≥ 3 years. The mean (± SD) follow-up duration for all censored lesions (stable disease and responding lesions) was 20.7 ± 19.4 months (range 12 days to 6.1 years).

Impact of Baseline Characteristics on Treatment Response

Table 4 summarizes the survival analyses assessing the impact of baseline characteristics on PFS-L.

Clinical Characteristics—Age ($p = 0.89$), primary tumor ($p = 0.17$), administration of systemic therapy ($p = 0.95$), and presence of neurological symptoms ($p = 0.47$) had no significant impact on PFS-L. Male sex showed a weak trend toward being a risk factor ($p = 0.13$). To test whether this trend was driven by an underlying survival benefit of breast tumor BMs, we compared breast BMs to other BMs and found no significant difference in PFS-L ($p = 0.76$). All three newly diagnosed BMs were LTRs, but the small sample size in this category did not allow us to statistically compare them with the recurrent BMs. In recurrent

lesions, time from the previous treatment was not a predictor of PFS-L (p = 0.60). Among 43 previously irradiated lesions, a previous surgical intervention did not impact PFS-L (p = 0.71). Pretreatment suspected diagnosis did not predict PFS-L (BMs vs uncertain/mixed vs RN, p = 0.77, log-rank test for trend; BMs and uncertain/mixed vs RN, p = 0.89).

Lesion Location—After visualizing the MNI map (Suppl. Fig. 2), lesion locations were categorized into four groups: lobar frontal (cortical/juxtacortical), lobar nonfrontal (cortical/juxtacortical), white matter, and deep gray matter or infratentorial. Lobar nonfrontal and white matter lesions tended to have worse prognoses than frontal, deep gray matter, and infratentorial lesions, but the differences were not statistically significant (p = 0.22; Table 4, Suppl. Fig. 2).

Lesion Size and Sphericity—Baseline tumor size measured as enhancing volume (CE_{vol}) was a predictor of PFS-L (p = 0.003), as the enhancing volume represented the best imaging surrogate of active tumor volume.[24] Every additional cubic centimeter of enhancing volume corresponded to an increased 40% risk of PD (HR 1.4). An optimal threshold of 2.5 cm^3 was found to best stratify lesions (adjusted p = 0.004), with $CE_{vol} \geq 2.5$ cm^3 bearing a 7.3-fold higher risk of progression (HR 7.3; Fig. 1A). The probability of PFS-L for lesions with $CE_{vol} < 2.5$ cm^3 was 86.8% at 6 months and remained unchanged (86.8%) at all the subsequent time points, until 6.1 years of follow-up (Fig. 1A).

Because CE_{vol} segmentation may be more demanding in clinical settings, we explored the value of whole-lesion volume as a marker of tumor size, including both the enhancing tissue and the central nonenhancing cystic/necrotic portions (when present). Whole-lesion volume showed a strong positive correlation with the enhancing volume (p < 0.0001, $R^2 = 0.94$, slope = 1.48; Suppl. Fig. 3A) and was also a predictor of PFS-L (p = 0.001, HR 1.3) with an optimal cutoff of 2.8 cm^3 (adjusted p = 0.010, HR 6.2).

Higher lesion sphericity predicted better PFS-L (p = 0.024, HR 0.02), and lesions with sphericity < 0.705 were 5.7 times more at risk for progression (adjusted p = 0.019, HR 5.7; Fig. 1C). The probability of PFS-L for sphericity ≥ 0.705 was 86.8% at 6 months and remained unchanged (86.8%) at all subsequent time points, until 4.1 years of follow-up (Fig. 1C).

CE_{vol} and sphericity showed only a weak inverse linear correlation (p = 0.009, $R^2 = 0.14$), suggesting these two radiological features may both have useful prognostic value (Suppl. Fig. 3B). In a bivariate Cox regression, CE_{vol} was a significant independent predictor of PFS-L (p = 0.03), while sphericity was not (p = 0.17). Based on the afore-mentioned analyses, we considered $CE_{vol} \geq 2.5$ cm^3 and sphericity < 0.705 as two risk factors and stratified lesions into the following risk groups: 1) no risk factors, 2) one risk factor (either $CE_{vol} \geq 2.5$ cm^3 or sphericity < 0.705), and 3) two risk factors.

These three groups had increasingly worse PFS-L (p < 0.0001, log-rank test for trend; Fig. 1E). Group 1 had significantly better PFS-L than group 2 (p = 0.004) and group 3 (p < 0.0001). The presence of one risk factor (group 2) and two risk factors (group 3) led to a risk of progression 10.9- and 51.7-fold higher, respectively. Conversely, the difference between

group 2 and group 3 was not significant (p = 0.17). The probability of PFS-L for lesions without risk factors (group 1) was 100% for the whole follow-up period up to 4.1 years (Fig. 1E), as no lesions belonging to this group progressed.

A high lesion sphericity also predicted complete ablation (p = 0.03), and small CE_{vol} tended to predict complete ablation (p = 0.11). Notably, a complete ablation was achieved in only 4 lesions with large CE_{vol} (≥ 2.5 cm^3), and in 50% of these (n = 2) the operators used two catheters.

Manually Computed Lesion Size and Sphericity—Because whole-lesion volume was strongly correlated with CE_{vol}, we explored the prognostic value of a size assessment through a single in-plane maximal axial diameter (d_{ax1}); d_{ax1} showed a strong direct correlation with CE_{vol} (p < 0.0001, R^2 = 0.75; Suppl. Fig. 3C) and was a predictor of PFS-L (p = 0.011). Every additional centimeter of maximal axial diameter corresponded to a 3.1-fold increased risk of PD (HR 3.1). An optimal threshold of ≥ 2 cm for d_{ax1} was found to stratify larger lesions with a 4.5-fold higher risk of PD (adjusted p = 0.035; HR 4.5; Fig. 1B). The probability of PFS-L for lesions with d_{ax1} < 2 cm was 86.5% at 6 months and 1 and 2 years, and 78.6% at 3 years, and remained unchanged (78.6%) at all subsequent time points, until 6.1 years of follow-up (Fig. 1B).

Similarly, we explored an approximated manually derived estimate of sphericity. Manually derived sphericity was not equivalent to the segmentation-derived sphericity (p = 0.45) and introduced a remarkable overestimation (moderate linear direct correlation, with p < 0.0001, R^2 = 0.48, slope = 0.18, and intercept = 0.79; Suppl. Fig. 3D). A logarithmic nonlinear regression best described the relationship between manually derived sphericity and sphericity (R^2 = 0.55). Manually derived sphericity predicted PFS-L (p = 0.043, HR < 0.01). An optimal cutoff of < 0.91 stratified low-sphericity lesions with a 3.3-fold higher risk of progression; however, this cutoff yielded a statistically nonsignificant p value after adjustment (p = 0.024, adjusted p = 0.092, HR = 3.3; Fig. 1D). The probability of PFS-L for lesions with manually derived sphericity ≥ 0.91 was 76.9% at 6 months and remained unchanged (76.9%) at all subsequent time points, until 6.1 years of follow-up (Fig. 1D).

When replicating the three risk groups using manual radiological risk factors d_{ax1} ≥ 2 cm and manually derived sphericity < 0.91, we obtained three groups with increasingly worse PFS-L (p = 0.0023, log-rank test for trend; Fig. 1F). Group 1 had significantly better PFS-L than group 2 (p = 0.0086) and group 3 (p = 0.005). The presence of one risk factor (group 2) and two risk factors (group 3) led to 6.4- and 7.2-fold higher risks of progression, respectively. Conversely, the difference between group 2 and group 3 was not significant (p = 0.63). The probability of PFS-L for lesions without risk factors (group 1) was 89.7% and remained unchanged (89.7%) at all subsequent time points, until 6.1 years of follow-up (Fig. 1F).

In the risk stratification based on manual measurements, 18 total lesions (38.2%) were reassigned to a different risk group compared with the segmentation-based stratification (Suppl. Fig. 4). In 18 cases, there were discrepancies between sphericity assessments (sphericity vs manually derived sphericity), and in 7 cases between size thresholds (CE_{vol} vs d_{ax1}). The reassignment in size risk categories was almost entirely attributable to a

more stringent optimal cutoff in the survival analysis based on manual measurement. Representative cases illustrating baseline size and sphericity influencing PFS-L after LITT are shown in Fig. 2.

Diffusion and Perfusion Imaging—Baseline DWI was available for all lesions. Median ADC ($p = 0.40$) and 10th percentile ADC ($p = 0.16$) did not predict PFS-L.

Baseline DSC was available for 43 lesions (91.5%). High median nrCBV tended to predict shorter PFS-L ($p = 0.09$, HR 2.2). High 90th percentile nrCBV, representing a marker of hotspots with higher vascularity, showed a stronger trend toward predicting shorter PFS-L ($p = 0.06$, HR 1.6). An optimized 90th percentile nrCBV cutoff of ≥ 2.5 was able to identify a subset of lesions (n = 7, 16.3%; Suppl. Fig. 5A) with highly perfused hotspots and worse PFS-L (adjusted $p = 0.010$, HR 5.6). The 90th percentile nrCBV was not correlated with CE_{vol} ($p = 0.18$, $R^2 = 0.04$; Suppl. Fig. 5B), but the 7 highly perfused lesions had larger size ($p = 0.011$, mean CE_{vol} 4.58 ± 3.25 vs 2.16 ± 1.37; Suppl. Fig. 5C). In addition, a visual evaluation of nrCBV maps revealed that in 4 cases (57.1%), the high perfusion hotspots were contaminated from cortical or vascular perfusion signal.

Histopathological Evaluations

Histopathological reports of the biopsy specimens obtained from the LITT catheter were available only for 13 lesions (27.7%). In 5 cases (38.5%), the evaluation highlighted malignant cells compatible with metastatic disease, whereas in the other 8 cases (61.5%), the evaluation showed treatment effects (RN)—including hyaline vasculopathy, reactive gliosis, and necrosis. The biopsy results did not predict PFS-L ($p = 0.14$), but sampling artifacts and the small population size may have affected this result. Confirmed BM (n = 5) was suspected as BM in 2 cases, as mixed/uncertain in 2 cases, and as RN in 1 case. Confirmed RN (n = 8) was suspected as RN in 2 cases, mixed/uncertain in 3 cases, and BM in 3 cases. This observation confirms that the BM/RN distinction based on imaging is challenging.

Discussion

In this study, we investigated the association between baseline clinical and radiological characteristics and recurrence after LITT in a cohort of 47 lesions from patients with BMs. To our knowledge, this is the first study that specifically evaluated all baseline pretreatment variables (including diffusion and perfusion MRI), the first to assess lesion sphericity, and the study with the longest follow-up duration after LITT treatment for BMs.

As a main finding, small size and spherical shape were proven to be the most relevant baseline features predicting PFS-L. The most likely interpretation of this result is that lesions with larger size and/or low sphericity are more likely to extend beyond the field of LITT treatment, and a radical ablation may be more challenging to achieve (Fig. 3). This interpretation is supported by the well-established idea that the extent of ablation is a predictor of LITT success[13,14,18,20,31] and by the observation that sphericity predicted the extent of ablation and size showed a trend toward predicting it. It is worth noting that evaluating the extent of ablation is inherently challenging because both the ablated and nonablated lesion portion enhance on postoperative T1-weighted images. Using subtraction

images helps in identifying a rim of additional nonlesional ablated tissue that only enhances after treatment and serves as a warranty of supratotal ablation. This methodology has relevant limitations, including its qualitative and conservative features, underestimating complete ablations in the absence of a well-demarcated ablation rim involving nonlesional tissue. This is a probable explanation for the low incidence of complete ablations in our cohort and the nonsignificant association between lesion size and extent of ablation.

A large baseline tumor size had already been reported as a risk factor for recurrence after LITT.[14,15,18] Bastos et al.[14] proposed a cutoff of 6 cc because it correlated with the extent of ablation, while Salehi et al.[18] used a cutoff of 5.6 cm^3, which was the median size of the lesions included in their cohort. We proposed a much stricter optimized cutoff of 2.5 cm^3 of CE_{vol} as highlighted by T1 subtraction maps,[24] and we demonstrated a substantial benefit in PFS-L for lesions < 2.5 cm^3. Alternatively, we validated a manual cutoff of < 2 cm for the maximal d_{ax1}, which served as an easier-to-obtain size estimate. While the probability of PFS-L at 6 months (70.6%) for our whole cohort was comparable to the probability reported in the literature (mean 59.7% ± 13.1% across studies),[6,13,14,16-18,20,22,32,33] lesions smaller than the optimized cutoffs had a higher probability of PFS-L: 86.8% (< 2.5 cm^3) and 86.5% (< 2 cm), respectively. Notably, the penetration in biological tissue of Nd:YAG lasers with wavelengths of 1064 nm is estimated up to 1 cm,[34] which is consistent with our proposed cutoff diameter of 2 cm (radius 1 cm).

This is the first study demonstrating that low sphericity is a risk factor for recurrence after LITT, and lesions with a segmentation-based sphericity ≥ 0.705 had a higher probability of PFS-L (86.8%) at 6 months. We proposed a manual estimate of sphericity, which was also a predictor of PFS-L, and lesions with manually estimated sphericity ≥ 0.91 had a longer PFS-L (e.g., 76.9% probability of PFS-L at 6 months). However, this PFS-L benefit in the log-rank analysis was not statistically significant after p value adjustment. Furthermore, manually estimated sphericity highly overestimated sphericity and caused multiple lesions to be reassigned when comparing groups according to risk factors. These results advocate for the usefulness of manually estimated sphericity, but we believe that the segmentation-based assessment yields more reliable sphericity measurements. It is worth mentioning that the depth of the catheter can be adjusted during the procedure to dispense laser treatment in multiple points along the catheter trajectory. Therefore, lesions with a more elongated shape may also be covered by the treatment field if the trajectory is aligned with the major axis of the lesion (optimal trajectory). However, an optimal trajectory is often not feasible due to eloquent tissue or vessels that must be preserved. Overall, a more spherical lesion is easier to treat because there is no major axis and multiple trajectories are equivalent.

In a bivariate Cox analysis on lesion size and sphericity, only the former represented an independent predictor of PFS-L. However, sphericity only weakly correlated with CE_{vol}, and lesion repartition in risk groups showed a cumulative protective effect of small size and high sphericity (group 1). Group 1 had a PFS-L probability of 100% for the entire 4 years of follow-up. Similarly, lesions belonging to group 1 according to manual measurements (d_{ax1} and manually estimated sphericity) had a higher probability of PFS-L (89.7% at 6 months, maintained at 6 years). Notably, the presence of any risk factors (large size and/or low sphericity, measured from segmentations or manually) yielded a significantly worse

prognosis, while a cumulative effect of the risk factors was not seen, as no statistical differences emerged from the group 2 versus group 3 comparison.

This is the first study to assess baseline diffusion and DSC perfusion metrics (ADC and nrCBV, respectively) as predictors of PFS-L after LITT. Although low ADC and high nrCBV are known as markers of aggressiveness in neuro-oncology,[35] they failed to predict PFS-L in a Cox proportional hazards regression analysis. A subset of lesions with highly perfused hotspots (90th percentile nrCBV ≥ 2.5) showed significantly worse PFS-L, but this result may have been confounded by an underlying larger tumor size in this group and by contamination of the perfusion signal from cortical and vascular voxels in some of these cases. A previous study[33] reported that high postprocedural dynamic contrast-enhanced perfusion markers, but not at baseline, were predictive of LITT failure. Overall, we believe that further evidence is needed to confirm the potential role of perfusion imaging in patient selection for LITT.

Lesion location showed some nonsignificant trends, with lobar frontal lesions and deep gray matter or infratentorial lesions being less at risk for progression than lobar nonfrontal and white matter locations. While the PFS-L benefit of deep gray matter and infratentorial lesions is not convincing due to the very small sample size with a long follow-up in this group, we believe that the different trends between white matter and cortical locations and between frontal and nonfrontal locations deserve further assessment in future studies.

Clinical variables such as symptoms at baseline, time from previous treatment, or primary tumor were not significant predictors of PFS-L. However, all newly diagnosed lesions were LTRs, suggesting the LITT success rate could potentially be higher in this cohort, although the small sample size did not allow us to test this hypothesis.

Limitations of the Study

Limitations of this study include its retrospective design and relatively small sample size. A factor we were not able to account for entirely is the lesion type, i.e., recurrent BMs versus RN. No significant difference was seen in our cohort according to histopathological diagnosis, but this result was possibly influenced by the small sample size in the group with biopsies because it has been established that lesion type is a variable influencing PFS after LITT.[6,14,17] Nevertheless, it should be noted that lesion type is not a known variable at the time of patient selection because the imaging distinction is unreliable,[5,36] and that LITT is a valid treatment for both BMs and RN.[4,17,19-22] Therefore, our results are valid in the setting of patient selection, when the clinician is unaware of the histopathological diagnosis. In addition, it should be noted that histopathological results from biopsies should be considered highly specific for recurrent BMs, but not sensitive. In fact, sampling artifacts may underestimate the presence of tumor cells within the lesion, especially considering that cases with mixed RN and tumor cells are reportedly not rare.[5]

Conclusions

This retrospective study demonstrated that small size and high sphericity are ideal baseline features for BMs considered for LITT treatment and should be assessed during the patient

selection phase. The presence of such features granted a PFS-L benefit, with cumulative effects when both features were present. These results suggest that size can be effectively assessed with either a segmentation-based or manual assessment, while for sphericity a segmentation-based approach should be preferred. Baseline diffusion imaging should not be used for patient selection, while the role of high-perfusion hotspots to identify lesions at risk for progression after LITT remains to be confirmed.

Supplementary Material

Refer to Web version on PubMed Central for supplementary material.

Acknowledgments

We are thankful to (in alphabetical order) Nicoletta Anzalone, Stefano Bastianello, Antonella Castellano, Eduardo Caverzasi, Gian Marco Conte, Andrea Falini, Anna Pichiecchio, Valentina Pieri, and Jingwen Yao for the fruitful discussion about our results. Dr. Cho received a training grant (no. T32 GM008042) from the National Institute of General Medical Sciences at NIH. This work was supported by the following grants: NIH/NCI R01CA270027, NIH/NCI R01CA279984, NIH/NCI P50CA211015.

ABBREVIATIONS

ADC	apparent diffusion coefficient
BM	brain metastasis
CET1	contrast-enhanced T1-weighted images
CE_{vol}	volume of the contrast-enhancing lesion
d_{ax1}	maximal diameter in the axial plane
d_{ax2}	maximal perpendicular diameter in the axial plane
d_{vert}	maximal vertical diameter (perpendicular to the axial slices)
DSC	dynamic susceptibility contrast
DWI	diffusion-weighted imaging
HR	hazard ratio
LITT	laser interstitial thermal therapy
LTDC	long-term disease control
LTR	long-term responder
mRANO	modified Response Assessment in Neuro-Oncology
Nd:YAG	neodymium-doped yttrium aluminum garnet
nrCBV	normalized relative cerebral blood volume
PD	progressive disease

PFS-L	lesion-specific progression-free survival
RN	radiation necrosis
RT	radiation therapy
SRS	stereotactic radiosurgery

References

1. Vogelbaum MA, Brown PD, Messersmith H, et al. Treatment for brain metastases: ASCO-SNO-ASTRO guideline. J Clin Oncol. 2022;40(5):492–516. [PubMed: 34932393]
2. Chen WC, Baal UH, Baal JD, et al. Efficacy and safety of stereotactic radiosurgery for brainstem metastases: a systematic review and meta-analysis. JAMA Oncol. 2021;7(7):1033–1040. [PubMed: 33983393]
3. Minniti G, Scaringi C, Paolini S, et al. Single-fraction versus multifraction (3 × 9 Gy) stereotactic radiosurgery for large (>2 cm) brain metastases: a comparative analysis of local control and risk of radiation-induced brain necrosis. Int J Radiat Oncol Biol Phys. 2016;95(4):1142–1148. [PubMed: 27209508]
4. Chen C, Lee I, Tatsui C, Elder T, Sloan AE. Laser interstitial thermotherapy (LITT) for the treatment of tumors of the brain and spine: a brief review. J Neurooncol. 2021;151(3):429–442. [PubMed: 33611709]
5. Medvid R, Ruiz A, Komotar RJ, et al. Current applications of MRI-guided laser interstitial thermal therapy in the treatment of brain neoplasms and epilepsy: a radiologic and neurosurgical overview. AJNR Am J Neuroradiol. 2015;36(11):1998-2006. [PubMed: 26113069]
6. Hong CS, Deng D, Vera A, Chiang VL. Laser-interstitial thermal therapy compared to craniotomy for treatment of radiation necrosis or recurrent tumor in brain metastases failing radiosurgery. J Neurooncol. 2019;142(2):309–317. [PubMed: 30656529]
7. Torres-Reveron J, Tomasiewicz HC, Shetty A, Amankulor NM, Chiang VL. Stereotactic laser induced thermotherapy (LITT): a novel treatment for brain lesions regrowing after radiosurgery. J Neurooncol. 2013;113(3):495–503. [PubMed: 23677747]
8. Sugiyama K, Sakai T, Fujishima I, Ryu H, Uemura K, Yokoyama T. Stereotactic interstitial laser-hyperthermia using Nd-YAG laser. Stereotact Funct Neurosurg. 1990;54-55:501-505. [PubMed: 2080375]
9. Damante MAJ Jr, Wang JL, Elder JB. Surgical management of recurrent brain metastasis: a systematic review of laser interstitial thermal therapy. Cancers (Basel). 2022;14(18):4367. [PubMed: 36139527]
10. Salem U, Kumar VA, Madewell JE, et al. Neurosurgical applications of MRI guided laser interstitial thermal therapy (LITT). Cancer Imaging. 2019;19(1):65. [PubMed: 31615562]
11. Lagman C, Chung LK, Pelargos PE, et al. Laser neurosurgery: a systematic analysis of magnetic resonance-guided laser interstitial thermal therapies. J Clin Neurosci. 2017;36:20–26. [PubMed: 27838155]
12. Rieke V, Butts Pauly K. MR thermometry. J Magn Reson Imaging. 2008;27(2):376–390. [PubMed: 18219673]
13. Carpentier A, McNichols RJ, Stafford RJ, et al. Laser thermal therapy: real-time MRI-guided and computer-controlled procedures for metastatic brain tumors. Lasers Surg Med. 2011;43(10):943–950. [PubMed: 22109661]
14. Bastos DCA, Rao G, Oliva ICG, et al. Predictors of local control of brain metastasis treated with laser interstitial thermal therapy. Neurosurgery. 2020;87(1):112–122. [PubMed: 31539421]
15. Beechar VB, Prabhu SS, Bastos D, et al. Volumetric response of progressing post-SRS lesions treated with laser interstitial thermal therapy. J Neurooncol. 2018;137(1):57–65. [PubMed: 29204838]

16. Rao MS, Hargreaves EL, Khan AJ, Haffty BG, Danish SF. Magnetic resonance-guided laser ablation improves local control for postradiosurgery recurrence and/or radiation necrosis. Neurosurgery. 2014;74(6):658–667. [PubMed: 24584138]
17. Ahluwalia M, Barnett GH, Deng D, et al. Laser ablation after stereotactic radiosurgery: a multicenter prospective study in patients with metastatic brain tumors and radiation necrosis. J Neurosurg. 2018;130(3):804–811. [PubMed: 29726782]
18. Salehi A, Kamath AA, Leuthardt EC, Kim AH. Management of intracranial metastatic disease with laser interstitial thermal therapy. Front Oncol. 2018;8:499. [PubMed: 30430083]
19. Sujijantarat N, Hong CS, Owusu KA, et al. Laser interstitial thermal therapy (LITT) vs. bevacizumab for radiation necrosis in previously irradiated brain metastases. J Neurooncol. 2020;148(3):641–649. [PubMed: 32602021]
20. Luther E, McCarthy D, Shah A, et al. Radical laser interstitial thermal therapy ablation volumes increase progression-free survival in biopsy-proven radiation necrosis. World Neurosurg. 2020;136:e646–e659. [PubMed: 32001408]
21. Sankey EW, Grabowski MM, Srinivasan ES, et al. Time to steroid independence after laser interstitial thermal therapy vs medical management for treatment of biopsy-proven radiation necrosis secondary to stereotactic radiosurgery for brain metastasis. Neurosurgery. 2022;90(6):684–690. [PubMed: 35311745]
22. Chaunzwa TL, Deng D, Leuthardt EC, et al. Laser thermal ablation for metastases failing radiosurgery: a multicentered retrospective study. Neurosurgery. 2018;82(1):56–63. [PubMed: 28419284]
23. Leu K, Boxerman JL, Cloughesy TF, et al. Improved leakage correction for single-echo dynamic susceptibility contrast perfusion MRI estimates of relative cerebral blood volume in high-grade gliomas by accounting for bidirectional contrast agent exchange. AJNR Am J Neuroradiol. 2016;37(8):1440-1446. [PubMed: 27079371]
24. Ellingson BM, Kim HJ, Woodworth DC, et al. Recurrent glioblastoma treated with bevacizumab: contrast-enhanced T1-weighted subtraction maps improve tumor delineation and aid prediction of survival in a multicenter clinical trial. Radiology. 2014;271(1):200–210. [PubMed: 24475840]
25. Ellingson BM, Wen PY, Cloughesy TF. Modified criteria for radiographic response assessment in glioblastoma clinical trials. Neurotherapeutics. 2017;14(2):307–320. [PubMed: 28108885]
26. Lin NU, Lee EQ, Aoyama H, et al. Response assessment criteria for brain metastases: proposal from the RANO group. Lancet Oncol. 2015;16(6):e270–e278. [PubMed: 26065612]
27. Sanvito F, Palesi F, Rognone E, et al. Impact of the inversion time on regional brain perfusion estimation with clinical arterial spin labeling protocols. MAGMA. 2022;35(3):349–363. [PubMed: 34643853]
28. Ellingson BM, Gerstner ER, Smits M, et al. Diffusion MRI phenotypes predict overall survival benefit from anti-VEGF monotherapy in recurrent glioblastoma: converging evidence from phase II trials. Clin Cancer Res. 2017;23(19):5745–5756. [PubMed: 28655794]
29. Cho NS, Hagiwara A, Eldred BSC, et al. Early volumetric, perfusion, and diffusion MRI changes after mutant isocitrate dehydrogenase (IDH) inhibitor treatment in IDH1-mutant gliomas. Neurooncol Adv. 2022;4(1):vdac124. [PubMed: 36033919]
30. Lausen B, Schumacher M. Evaluating the effect of optimized cutoff values in the assessment of prognostic factors. Comput Stat Data Anal. 1996;21(3):307–326.
31. Ali MA, Carroll KT, Rennert RC, et al. Stereotactic laser ablation as treatment for brain metastases that recur after stereotactic radiosurgery: a multiinstitutional experience. Neurosurg Focus. 2016;41(4):E11.
32. Hawasli AH, Bagade S, Shimony JS, Miller-Thomas M, Leuthardt EC. Magnetic resonance imaging-guided focused laser interstitial thermal therapy for intracranial lesions: single-institution series. Neurosurgery. 2013;73(6):1007–1017. [PubMed: 24056317]
33. Traylor JI, Bastos DCA, Fuentes D, et al. Dynamic contrast-enhanced MRI in patients with brain metastases undergoing laser interstitial thermal therapy: a pilot study. AJNR Am J Neuroradiol. 2019;40(9):1451–1457. [PubMed: 31371353]
34. Mensel B, Weigel C, Hosten N. Laser-induced thermotherapy. Recent Results Cancer Res. 2006;167:69–75. [PubMed: 17044297]

35. Sanvito F, Castellano A, Falini A. Advancements in neuroimaging to unravel biological and molecular features of brain tumors. Cancers (Basel). 2021;13(3):424. [PubMed: 33498680]

36. Patel PD, Patel NV, Davidson C, Danish SF. The role of MRgLITT in overcoming the challenges in managing infield recurrence after radiation for brain metastasis. Neurosurgery. 2016;79(suppl 1):S40–S58. [PubMed: 27861325]

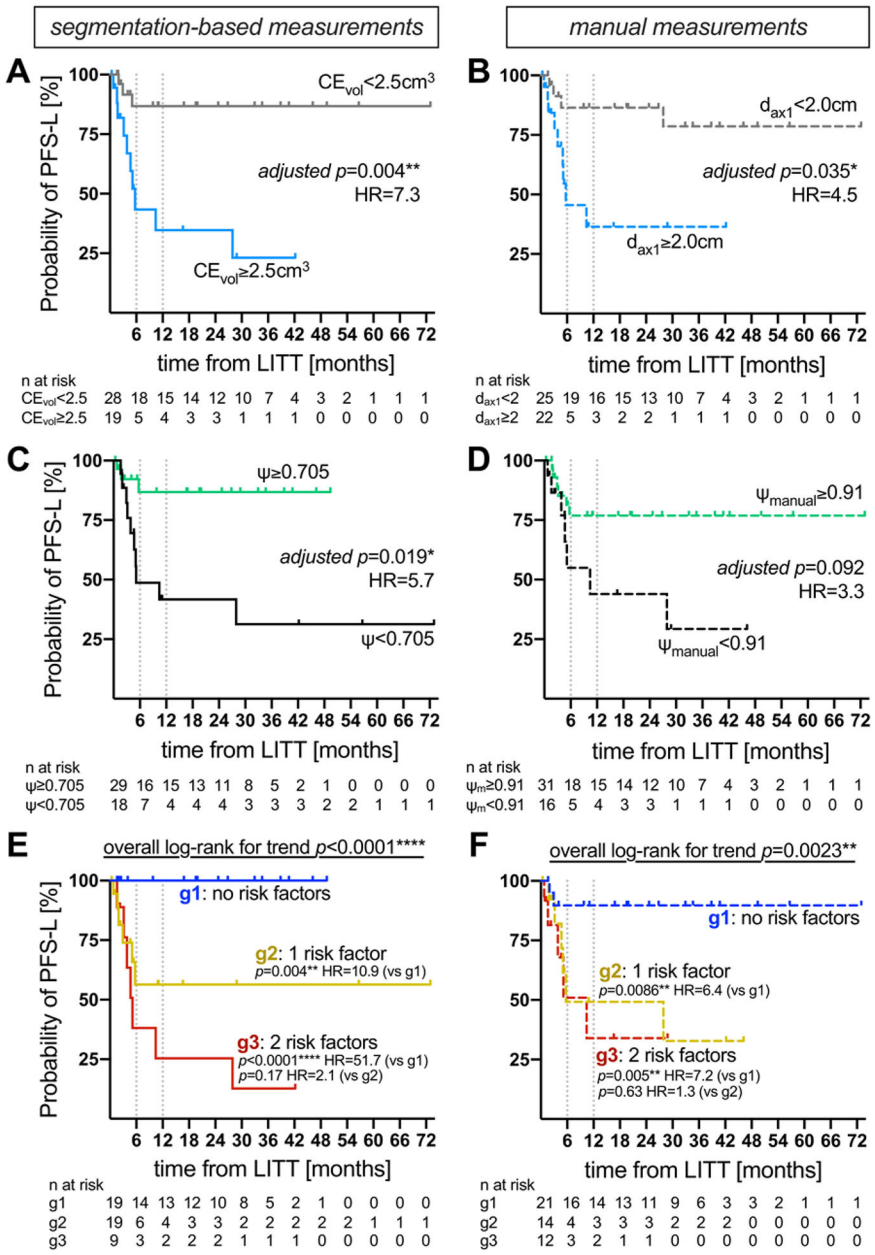

FIG. 1.

Kaplan-Meier curves representing the probability of PFS-L of groups stratified according to optimal cutoffs. Small size, measured as either enhancing volume (**A**) or maximal axial manual diameter (**B**), was a positive prognostic factor, as well as high sphericity, measured either from the segmented lesion (**C**) or through manual diameters (**D**). Three risk groups (**E and F**) were identified depending on the presence of 0, 1, or 2 of the abovementioned risk factors (large size and low sphericity). *p < 0.05; **p < 0.01; ****p < 0.0001. g1 = group 1, g2 = group 2, g3 = group 3.

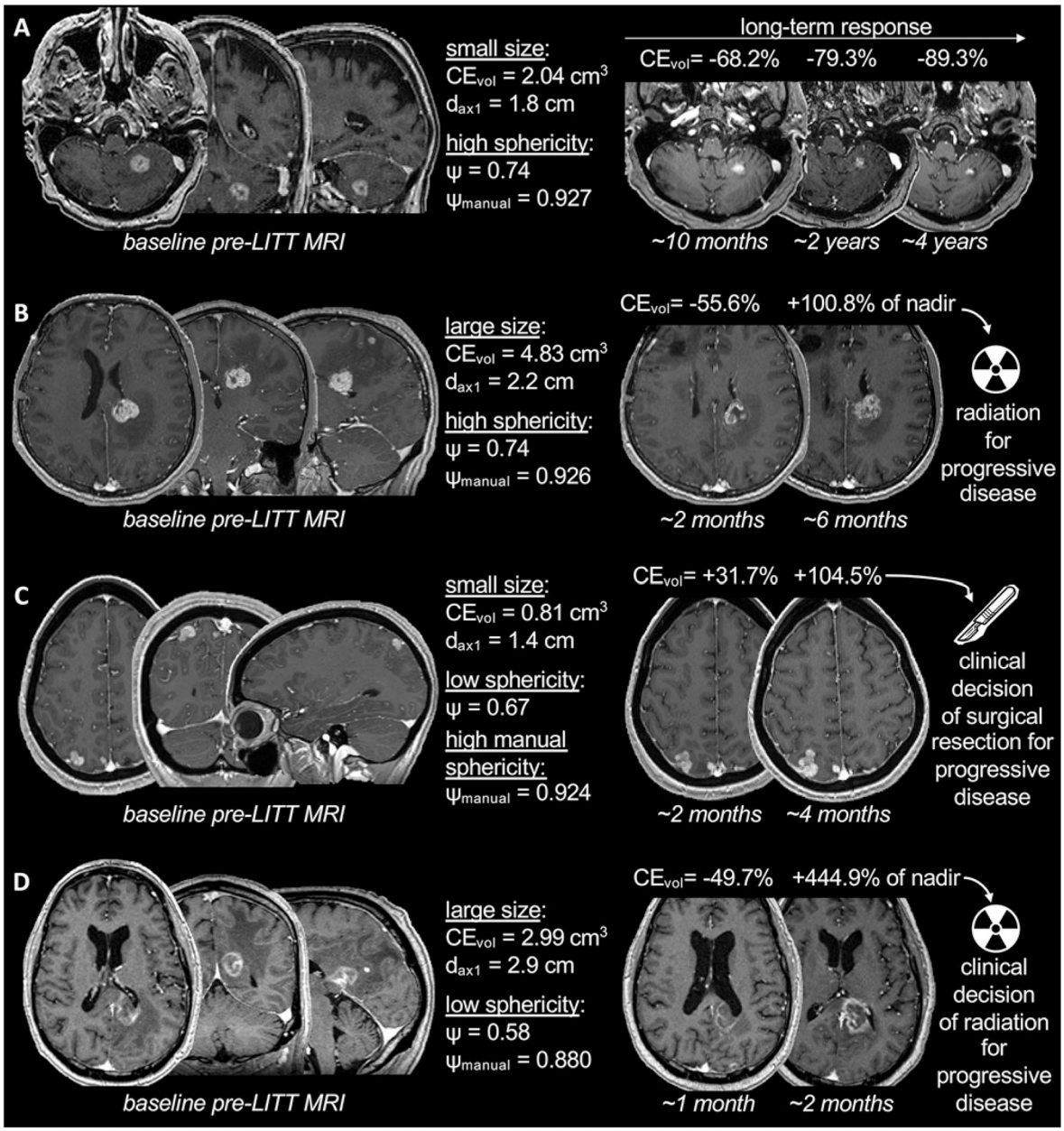

FIG. 2.

Representative cases. **A:** Images obtained in a 58-year-old male with a left cerebellar lesion (primary: melanoma) recurring approximately 1 year after SRS. The lesion shows small size and high sphericity (no risk factors) and LITT achieved a long-term response, sustained after 4 years. **B:** Images obtained in a 40-year-old male with a left hemispheric lesion (primary: kidney) involving the corpus callosum and centrum semiovale, recurring approximately 2 years after SRS. The lesion exhibited large size (remarkably beyond the proposed cutoffs) and high sphericity (one risk factor) and progressed 6 months after LITT. **C:** Images obtained in a 36-year-old female with a right parietal lesion (primary: sarcoma) recurring approximately 3 years after SRS. Despite its very small size, the lesion had low sphericity (it was irregularly shaped, as apparent; one risk factor) and progressed 4 months

after LITT. Notably, the low sphericity was only captured through the segmentation-based approach as opposed to the manual approach. **D:** Images obtained in a 63-year-old male with a left corpus callosum lesion (primary: melanoma) recurring approximately 6 months after SRS. The lesion exhibited a large size and low sphericity (two risk factors) and regrew at a very fast pace within 2 months after LITT.

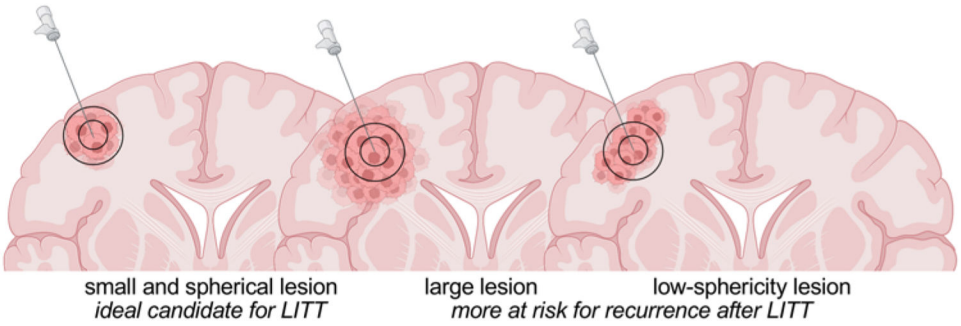

FIG. 3.

Schematic representation of the two main risk factors for LITT failure. Our interpretation is that large lesions and nonspherical lesions may be more challenging to entirely cover with the LITT treatment field, and therefore are more at risk for progression/recurrence.

TABLE 1.

Demographic and clinical baseline characteristics for each lesion (n = 47) and corresponding patient (n = 42)

Baseline Characteristic	Value
Mean age ± SD, yrs	58.0 ± 13.9
Sex, n (%)	
Male	25 (53.2)
Female	22 (46.8)
Primary tumor, n (%)*	
Breast	7 (14.9)
Lung	21 (44.7)
Kidney or urinary tract	5 (10.6)
Melanoma	8 (17.0)
Other	6 (12.8)
Tongue (SCC)	2 (4.3)
GI tract	2 (4.3)
Lower-limb sarcoma	1 (2.1)
Salivary glands	1 (2.1)
Symptoms at LITT time, n (%)	
Symptomatic	29 (61.7)
Asymptomatic	18 (38.3)
Suspected diagnosis, n (%)	
BM	21 (44.7)
RN	19 (40.4)
Uncertain/mixed	7 (14.9)
Prior local treatment	
Newly diagnosed, n (%)	3 (6.4)
Recurrent, n (%)	44 (93.6)
S/P surgery	10 (21.3)
S/P radiation	43 (91.5)
Mean mos from treatment ± SD†	16.0 ± 11.6
Systemic therapy, n (%)‡	
Chemotherapy	9 (19.1)
Targeted therapy	16 (34.0)
Immunotherapy	10 (21.3)
Antiangiogenetic	3 (6.4)
Hormonal therapy	1 (2.1)
None	11 (23.4)
Unknown	3 (6.4)

GI = gastrointestinal; SCC = squamous cell carcinoma; S/P = status post.

[*] This grouping of primary tumor categories (lung, breast, kidney or urinary tract, melanoma, and other) is the one applied to survival analyses. Further details on histotypes and molecular profiles can be found in Suppl. Table 1.

[†] For recurrent lesions only.

[‡] Systemic therapy from 3 months before to 3 months after LITT; many lesions received combination schemes.

TABLE 2.

Baseline radiological characteristics for each lesion (n = 47)

Baseline MRI Characteristic	Value
Lesion location, n (%) *	
Frontal	10 (21.3)
Parietal	10 (21.2)
Temporal	2 (4.3)
Occipital	6 (12.8)
Cingulate	2 (4.3)
Deep gray matter	3 (6.4)
White matter	11 (23.4)
Cerebellum	2 (4.3)
Brainstem	1 (2.1)
Mean size ± SD	
Enhancing volume (CE_{vol}), cm^3	2.68 ± 1.96
Manual diameter (d_{ax1}), cm	2.1 ± 0.6
Mean sphericity ± SD	
Segmentation-based	0.70 ± 0.12
Manual	0.91 ± 0.03
Mean cohort diffusion MRI ± SD	
Median lesion ADC, × 10^{-3} mm^2/sec	1.24 ± 0.18
10th percentile lesion ADC, × 10^{-3} mm^2/sec	0.95 ± 0.16
Mean cohort perfusion MRI ± SD	
Median lesion nrCBV	0.89 ± 0.51
90th percentile lesion nrCBV	1.72 ± 0.92
Mean days from MRI to LITT ± SD	15.7 ± 13.3

* Deep gray matter includes the thalamus and basal ganglia; white matter includes the corpus callosum and centrum semiovale.

TABLE 3.

Treatment response assessment according to PFS-L

Treatment Response Category	No. of Lesions (%)	Mean FU Duration ± SD (mos)
Responding		
LTR (≥12 mos)	15 (31.9)	36.0 ± 14.4
FU <12 mos	2 (4.3)	11.0 ± 0.1
PD		
Early PD (<6 mos)	11 (23.4)	3.3 ± 1.7
Late PD (6–12 mos)	1 (2.1)	10.7
Stable disease		
LTDC (≥12 mos)	4 (8.5)*	32.2 ± 16.7
FU 6–12 mos	1 (2.1)	9.8
FU <6 mos	13 (27.7)	2.4 ± 1.5

FU = follow-up.

*Including n = 1 PD at 28 months.

TABLE 4.

Treatment response predictors at baseline

Baseline Variable	p Value	HR (95% CI)*
Age	0.89	
Male sex	0.13	2.4 (0.8–7.1)
Primary tumor	0.17	
Breast vs all	0.76	
Neurological symptoms	0.47	
Time from treatment†	0.60	
Previous surgery†	0.71	
Systemic therapy	0.95	
Suspected diagnosis	0.77	
BM/uncertain vs RN	0.89	
Lesion location	0.22	
DGM/IT vs LF	0.57	
DGM/IT vs LNF	0.14	3.5 (0.7–19)
DGM/IT vs WM	0.06	7.7 (0.9–66)
LF vs LNF	0.16	2.7 (0.7–11)
LF vs WM	0.11	4.3 (0.7–27)
LNF vs WM	0.92	
CE_{vol} continuous, cm^3	0.003	1.4 (1.1–1.8)
CE_{vol} ≥2.5 cm^3	0.004‡	7.3 (2.3–24)
Whole-lesion volume, cm^3	0.001	1.3 (1.1–1.5)
Whole volume ≥2.8 cm^3	0.010‡	6.2 (2–20)
Sphericity	0.024	0.02 (0–0.6)
Sphericity <0.705	0.019‡	5.7 (1.9–18)
Manual diameter (d_{ax1}), cm	0.011	3.1 (1.3–7)
d_{ax1} ≥2	0.035‡	4.5 (1.4–14)
Manually derived sphericity	0.043	<0.01 (0–0.7)
Manually derived sphericity <0.91	0.092‡	3.3 (0.95–11)
Median ADC	0.40	
10th percentile ADC	0.16	
Median nrCBV	0.09	2.2 (0.9–5)
90th percentile nrCBV	0.06	1.6 (0.98–3)
90th nrCBV ≥2.5	0.010‡	5.6 (0.7–44)

DGM/IT = deep gray matter or infratentorial; LF = lobar frontal (cortical/juxtacortical); LNF = lobar nonfrontal (cortical/juxtacortical); WM = white matter.

*HRs are reported only if the p value is significant or trends toward significance.

[†] For recurrent lesions only.

[‡] After adjustment for simultaneous testing.